Electronic structures and magnetic moments of $Fe_{3+y}Si_{1-y}$ and $Fe_{3-x}V_xSi$ alloys with DO_3-derived structure

J. Kudrnovský,* N. E. Christensen,† and O. K. Andersen
Max-Planck-Institut für Festkörperforschung, Heisenbergstrasse 1, D-7000 Stuttgart 80, Federal Republic of Germany
(Received 17 August 1990)

We present *ab initio* calculations of magnetic moments and local electronic densities of states in binary $Fe_{3+y}Si_{1-y}$ and ternary $Fe_{3-x}V_xSi$ random alloys with DO_3-derived structures. The local-spin-density approximation, the linear muffin-tin orbital method, and the coherent-potential approximation (LMTO-CPA) were used. In $Fe_{3+y}Si_{1-y}$ the excess (as compared to Fe_3Si) Fe atoms occupy the Si[D] sites of the Fe_3Si host and create a strong d scattering. A realistic-alloy calculation thus requires the application of the CPA. In both types of alloys the moments of Fe atoms occupying the B sites remain essentially unchanged when the concentrations (y in $Fe_{3+y}Si_{1-y}$, x in $Fe_{3-x}V_xSi$) are varied. The Fe[A,C] moments vary almost linearly with y and x, in agreement with experimental observations. The sublattice density-of-states functions provide insight into the site preference for substitutional transition-metal impurities in Fe_3Si.

I. INTRODUCTION

Experimental and theoretical investigations of Fe_3X (X=Al, Si, Ga) compounds have revealed a number of interesting physical properties. For example, it appears that transition-metal impurities enter the lattice substitutionally with a remarkable site preference. Also, certain systematic behaviors of the sublattice magnetic moments when the impurity concentrations are varied have been found, and a simple rule expressed as the so-called "local-environment model" has been deduced. Details of the experimental findings were reviewed in Ref. 1. We shall describe here the results of *ab initio*, spin-polarized electronic-structure calculations for two types of alloys in this class, $Fe_{3+y}Si_{1-y}$ and $Fe_{3-x}V_xSi$.

The compounds considered here form DO_3-related structures.[1,2] The (ordered) Fe_3Si crystallizes in the DO_3 structure, which may be viewed as a fcc Bravais lattice with a basis consisting of four atoms, types A, B, C, and D, associated with each lattice point as illustrated in Fig. 1. Disregarding differences between A, B, C, and D atoms, their positions define a bcc lattice with half the lattice constant. The DO_3 structure may then be considered as being made up of four fcc sublattices, A, B, C, and D, arranged regularly along the body diagonal. Each A atom is at the center of a cube with four B and four D atoms at the corners in tetrahedral arrangements. Similarly, each B atom is at the center of a cube with four A and four C atoms at the corners. In Fe_3Si, Fe atoms occupy the A, C, and B sites. Thus, the Fe atoms on the (structurally and magnetically) equivalent A and C sites have tetrahedral point symmetry with four Fe[B] and four Si[D] atoms as nearest neighbors. The Fe atoms on the B sublattice have cubic point symmetry with eight Fe[A,C] atoms as nearest neighbors, just like in elemental bcc iron.

Polarized-neutron experiments,[3,4] as well as saturation magnetization measurements,[5] have established that the magnetic moments of the two types of Fe atoms are very different. The B-site moment in Fe_3Si, $m_{Fe[B]} \approx (2.2-2.4)\mu_B$, is close to the moment of elemental bcc Fe, while the moment on the A and C sites, $m_{Fe[A,C]} \approx (1.1-1.35)\mu_B$, is significantly smaller. A small, negative moment, $-0.07\mu_B$, was found on Si[D].

Silicon-iron alloys, $Fe_{1+x}Si_x$ exist[6] as a continuous range of solutions for x between 0 and 0.265. For Si contents between 10 and 25 %, the alloys form DO_3-related structures with the Si atoms preferentially occupying the

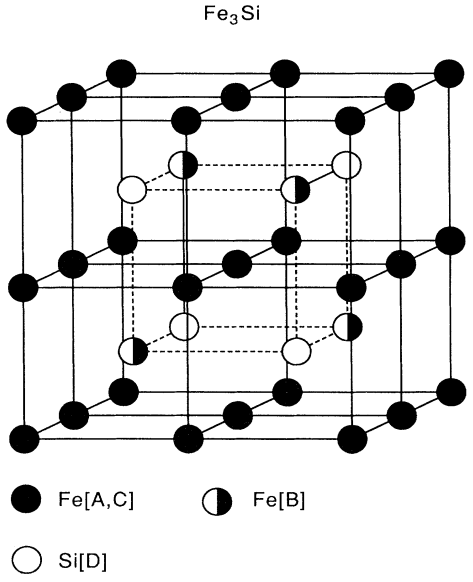

FIG. 1. Sketch of the DO_3 structure (Fe_3Si taken as an example). Solid circles, ●, Fe[A,C]; Open circles, ○, Si[D]; Half-solid circles, ◑, Fe[B].

D site, i.e., the sites where Si resides in the ordered Fe_3Si compound. The disordered, but DO_3-related, Fe-Si alloys of this type will be labeled as $Fe_{3+y}Si_{1-y}$, and they exist in the range $0.4 \leq y \leq 1.0$. The magnetic properties of these binary alloys are well described by the phenomenological model[1,7] in which the moment of Fe on A and C sites increase linearly with the average number of Fe atoms in their nearest-neighbor shell, where Fe atoms with increasing y replace Si. These extra Fe atoms are in the model considered as Fe[B]-type iron atoms, and over the entire y range it is assumed that the Fe[B] moments have the magnitude $2.20\mu_B$, the one of elemental bcc iron.

Thus, when an Fe atom enters the system, it replaces a Si[D] moment of $-0.07\mu_B$ by this large moment, $2.20\mu_B$. This local-environment model is also the basis for the interpretation[1,7] of the concentration-dependent magnetic behavior of $Fe_{3-x}T_xSi$ (T being a transition metal) alloys. In these alloys, iron atoms are replaced by another transition metal, e.g., V, Mn, Co, ... So far the local-environment model for the binary and ternary DO_3-related alloys described above has been justified by the fact that it explains trends in the observed total moments versus composition. We shall demonstrate, by means of *ab initio* electronic structure calculations within the local-spin-density approximation (LSDA) that the empirical rules also follow from a quantitative theory.

A unique property of Fe_3Si is that $3d$ transition-metal impurities selectively substitute Fe on one of the two inequivalent sites. Impurities of elements to the left of Fe in the Periodic Table (e.g., Mn or V) show a strong preference for B sites, whereas those to the right, such as Co or Ni, select the A or C sites. This site preference also occurs[1,2] in concentrated alloys like $Fe_{3-x}V_xSi$ and $Fe_{3+x}Mn_xSi$, where V or Mn substitute exclusively Fe[B] up to concentrations as high as $x=0.75$ (V case) or 0.5 (Mn case). Experimentally, these site-preference properties have been demonstrated by nuclear-magnetic-resonance[8] (NMR) neutron diffraction,[9] Mössbauer data,[10] and, most recently, by x-ray appearance near-edge studies (XANES) and extended x-ray-absorption fine-structure (EXAFS) studies.[11] We show in the present work that crude total-energy estimates for $Fe_{3-x}T_xSi$ alloys, requiring only the electronic structure of Fe_3Si, are able to explain this remarkable property.

The electronic structure of pure Fe_3Si was first studied theoretically by Switendick[12] who performed a non-spin-polarized augmented-plane-wave (APW) calculation, and subsequently included an empirical exchange splitting to account for the observed magnetic moments. Similar calculations were presented by Ishida *et al.*[13] for Fe_3Al. Williams *et al.*[14] performed *ab initio* self-consistent LSD calculations using the augmented-spherical-wave (ASW) method, and obtained iron moments, $1.36\mu_B$ on the A,C sites and $2.48\mu_B$ on the B sites, in good agreement with experiment. Theoretical studies of the electronic structures of impurities in Fe_3Si were carried out by Garba and Jacobs[15] who applied the recursion method based on an empirical tight-binding Hamiltonian. These calculations were not self-consistent, in contrast to the recent work by Ishida *et al.*[16] who performed LSD-LMTO (linear muffin-tin orbital) calculations with a supercell geometry modeling $Fe_{3-x}T_xGa$ (T=Cr, Mn . . .) alloys with $x=0.25$. We wish to proceed further by including, simultaneously, spin polarization and the effects of chemical disorder. We do this by performing calculations within the LSDA using the coherent-potential approximation (CPA) in conjunction with the linear muffin-tin orbital method in the tight-binding (TB) formulation. The CPA is known to reliably describe the electronic states in alloys, and allows us here to examine, contrary to the supercell approach, the electronic structures of $Fe_{3+x}Si_{1-y}$ and $Fe_{3-x}V_xSi$ alloys for any values of y and x. We have chosen $Fe_{3-x}V_xSi$ to represent the $Fe_{3-x}T_xSi$ alloys in this work for two reasons: (i) The V impurity is simpler to examine than, for example, Mn, because it is nonmagnetic. (ii) For $x>0.5$, Mn starts to occupy not only B sites but also A and C positions,[1,2] whereas the strong selectivity of V for the B sites remains[11] up to higher concentrations ($x \simeq 0.75$).

The outline of the rest of the paper is as follows: The principles of the LMTO-CPA alloy calculations are described in the following section. Before presenting the actual results of the CPA calculations for $Fe_{3+y}Si_{1-y}$ and $Fe_{3-x}V_xSi$ in Sec. IV, we briefly discuss (Sec. III) the electronic structure of the (ordered) Fe_3Si DO_3 crystal. This serves the purpose of describing the bonding characteristics and the features leading to the site selectivity of transition-metal impurities. Results of a detailed study of the magnetic properties, including pressure-induced high-spin to low-spin transitions in Fe_3Si, Fe_3Al, and Fe_2MnSi ordered compounds are presented elsewhere.[17] Summary and conclusions are given in Sec. V.

II. METHOD OF CALCULATIONS

The LMTO Hamiltonian in the orthonormal representation and in the atomic-sphere approximation (ASA) is[18]

$$H_{RL,R'L'}=C_{RL}\delta_{RR'}\delta_{L'L} + \Delta_{RL}^{1/2}[S^0(1-\gamma S^0)^{-1}]_{RL,R'L'}\Delta_{R'L'}^{1/2}, \quad (1)$$

where R runs over the sites of the four sublattices, and $L \equiv (l,m,\sigma)$ is the combined angular-momentum index, with σ being the spin index, $l \leq 2$ being the orbital and m the azimuthal quantum number. The Hamiltonian H is diagonal in the spin. The structure matrix $S^0_{RL,R'L'}$ is independent of the lattice constant and the spin, and it corresponds to the underlying bcc lattice. The scattering in channel L of the atom at site R is characterized by the potential parameters X_{RL} with $X=C$, Δ and γ giving,[18] respectively, the position, the width, and the shape of the resonance. The randomness enters the alloy Hamiltonian, Eq. (1), via the random potential parameters X_{RL}. Details concerning the LMTO-CPA can be found in Refs. 19 and 20. The generalization of the LMTO-CPA method from the simple-lattice case to the present case of four interpenetrating lattices is straightforward. We use sp^3d^5 orbitals on each atom so that our LMTO-CPA Hamiltonian, for each of the two spin directions, has the

dimension 36×36.

The $Fe_{3+y}Si_{1-y}$ as well as the $Fe_{3-x}V_xSi$ alloys can be treated, formally, as binary alloys, $\mathcal{A}_{1-c}\mathcal{B}_c$ formed by the two end-point crystals $\mathcal{A}$ and $\mathcal{B}$. In both cases, $\mathcal{A}$ is the ordered Fe_3Si, and the $\mathcal{B}$ crystal is, in the case of $Fe_{3+y}Si_{1-y}$, Fe_3Fe ($c=1$), whereas the $\mathcal{B}$ system for the other case is the Heusler-type Fe_2VSi alloy. The potential parameters for these end-point crystals were determined[17] from self-consistent LMTO-ASA calculations within the LSD approximation using the same atomic-sphere radius (2.608 a.u.) for all constituent atoms and both end-point crystals $\mathcal{A}$ and $\mathcal{B}$. This latter simplification is justified by the observation[21] that the lattice constant remains essentially unchanged when the alloy composition is varied. This way of choosing the potential parameters has the following advantages: (i) The choice is "exact" in the $\mathcal{A}$ and $\mathcal{B}$ limits: (ii) The potential of, say, the Fe[B] and V[B] are properly related to each other on the energy scale. These two points allow us, as a first approximation, to circumvent fully charge- and spin-self-consistency calculations for concentrations $0<c<1$. Our choice of end-point crystals leads effectively to concentration-dependent potential parameters of the Fe atoms on the A,C sublattices because the Fe[A,C] potentials are different in Fe_3Si and Fe_3VSi, and similarly, the Fe[A,C] potentials in Fe_3Si are different from those in Fe_3Fe. Thus, the potential parameters of Fe[A,C] fluctuate upon alloying between the limiting values of the end-point crystals. This is included in the CPA, and it leads to a dependence of the A,C potential parameters on the environment of these atoms. Note that this is the key feature of the phenomenological local-environment model.[1]

The coupled system of CPA equations for the four sublattices is solved for each spin direction ("up" and "down") in a manner that is similar to the calculation for the simpler fcc $Pd_{75}Fe_{25}$ alloy.[22] The energy-dependent quantities, like the density-of-states functions, are calculated with an energy resolution of 0.01 Ry. The k-space integrations are performed using a mesh corresponding to 110 points in the irreducible wedge of the fcc Brillouin zone. In order to keep the number of CPA iterations as low as possible, the calculations are performed with the energies shifted by 0.02 Ry along the imaginary axis in the complex plane. Once convergence is achieved, an analytical deconvolution back to the real axis is performed.[23] Having solved the CPA equation set, we calculate the total density of states (DOS) by summing the two spin contributions. The total DOS is then integrated, and the alloy Fermi level, E_F is determined from the known number of electrons. Finally, we integrate the sublattice "up"- and "down"-DOS functions to determine the sublattice magnetic moments.

III. ORDERED Fe_3Si AND Fe_2VSi

Before we present the results of our LMTO-CPA alloy calculations, we shall briefly examine the electronic structures of two of the end-point compounds, Fe_3Si and Fe_2VSi (that of bcc Fe is assumed to be well known[24–28]). This will be done by considering only the results of nonpolarized LMTO calculations, and the purpose is to demonstrate that the CPA calculations presented later contain the proper features of the end-point compound DOS functions, and further to discuss, on the simplest possible basis, what to expect from the more involved calculations. Also, we shall address here the site preference for substitutional transition-metal impurities.

We shall start by considering Fe_3Si. The Fe[A,C] and Fe[B] d DOS functions are shown in Figs. 2(a) and 2(b), respectively. In addition to the calculation of the d projected functions shown here, we have also projected the e_g and t_{2g} contributions separately (using a cubic-harmonic basis set). As mentioned earlier, Fe[B] is eightfold coordinated to Fe[A,C], and it is therefore not surprising that the Fe[B] projected DOS has a two-peak structure similar to what is found in bcc elemental Fe. Also, this implies that one must expect that spin polarization will produce an Fe[B] moment of the same order of magnitude ($2.2\mu_B$) as in bcc Fe. In fact, one finds[17] that the Fe[B] moment is close to $2.5\mu_B$. The two-peak structure in the Fe[B] DOS really consists of three peaks (identified by the cubic-harmonic projection), a low-lying t_{2g} peak of states bonding to the Fe[A,C] d orbitals, an essentially nonbonding e_g peak, and, on the high-energy side of the latter, the t_{2g} peak antibonding to the Fe[A,C] orbitals. The signature of an interaction between orbitals on the B site and orbitals on the [A,C] sites is the coincidence of structures in the Fe[B] and Fe[A,C] projected densities of states. Since the full Hamiltonian is diagonal in the spin, this holds separately for majority and minority bands. To a first approximation,[28] the shapes of the minority and majority bands are similar, but they will be displaced relatively to each other by a splitting given by mI, where m is the Fe[B] moment $2.5\mu_B$ and $I=0.06$ Ry is the Stoner parameter. The spin-polarized CPA calculations (the following section) also agrees with this. The moments on the Fe[A,C] sites, which are $\simeq1.2\mu_B$ (following section, Refs. 14, 17, and experiment[1]), are induced through the interaction with the Fe[B] majority- and minority-spin orbitals.

The characteristic difference between the "tetrahedral" Fe[A,C] and the "bcc" Fe[B] DOS, namely, the fact that the former has three main peaks whereas the latter has a two-peak structure, further enables us to understand the site preference for substitutional $3d$ transition-metal impurities in Fe_3Si. When an iron atom is replaced by a transition element with fewer d electrons than Fe, it is energetically more favorable to fill up the low-lying DOS peak of the "bcc" d DOS than filling states in the low-lying *and* the middle peak of the Fe[A,C] DOS. Consequently, such impurities will prefer to enter the B sites. On the other hand, a transition metal with more d electrons than Fe prefers to replace an [A,C] Fe atom because the energy associated with the filling of the two lowest peaks of the [A,C] Fe d DOS is lower than that of a structure where the high-lying second peak of the Fe[B] DOS becomes (partially) filled. These considerations are based on a comparison of total energies of different structures made on the basis of the sum of one-electron energies alone in the spirit of the "frozen-potential" method.[29] The Fe[A,C] and V DOS func-

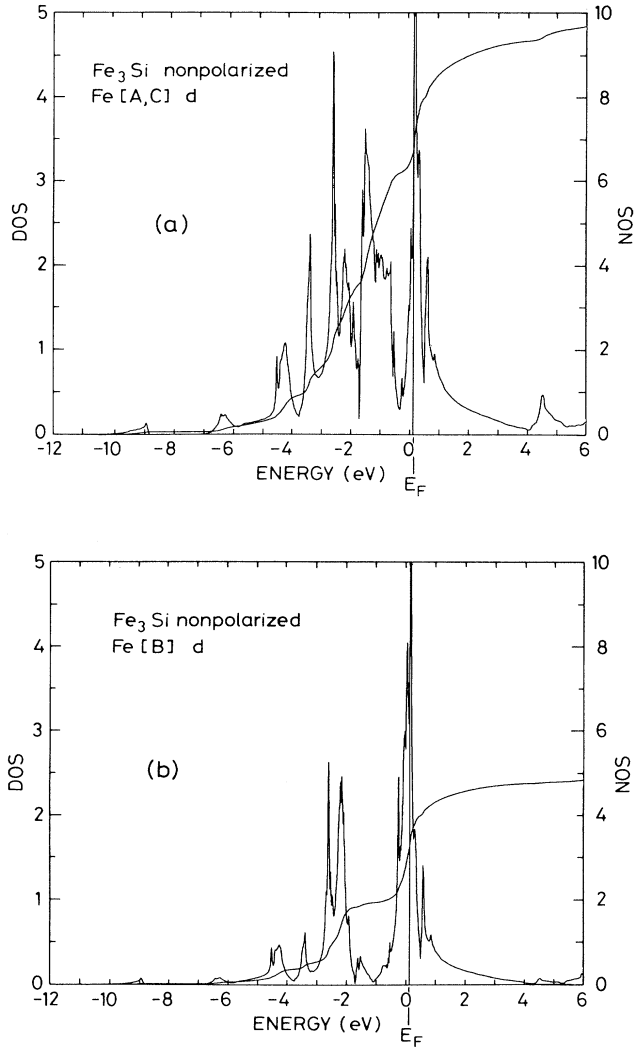

FIG. 2. Fe_3Si. (a) Fe[A,C]d density-of-states function calculated without spin polarization (Ref. 17). (b) same as (a) but for the B sites.

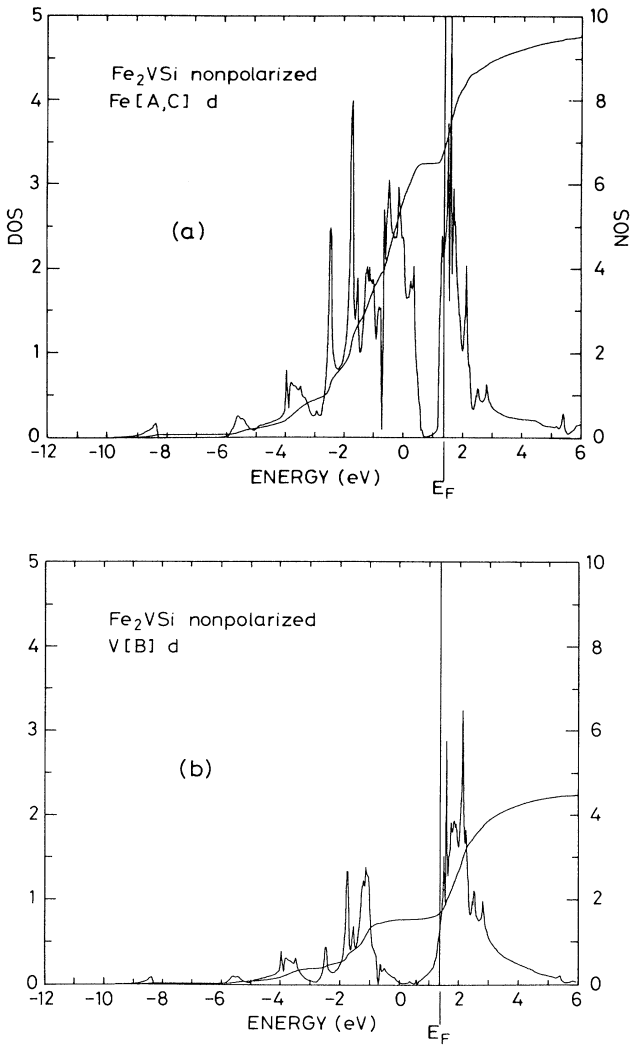

FIG. 3. Fe_2VSi. (a) Fe[A,C]d DOS. (b) V[B]d DOS.

tions, again calculated without spin polarization, are shown in Figs. 3(a) and 3(b). In this compound the Fe[B] atoms are completely substituted by V which has a higher-lying d-level position and more extended d orbitals. The V DOS has the typical two-peak structure of transition metals on the B sites, but, as in the case of Fe[B], the peak of t_{2g} states antibonding to Fe[A,C] is located on the high-energy side of the e_g nonbonding peak, i.e., again the apparent two-peak structure is really composed of three strong peaks. The bonding t_{2g} peak antibonding to Fe[A,C] is mostly Fe like and the antibonding t_{2g} peak is mostly V like. Contrary to the case of Fe[B], the effective exchange constant (I) for V is not large enough to spin polarize the e_g peak, and the weak antiferromagnetic moment is caused by the fact that the minority-spin Fe[A,C] level lies higher (by approximately 0.02 Ry), and, hence, closer to the V level than the majority-spin Fe[A,C] level. Consequently, the minority-spin bonding t_{2g} peak has many more weight on V than the majority-spin bonding t_{2g} peak. The Fe[A,C] moment in Fe_2VSi is small ($0.37\mu_B$, see next section) as compared to the $1.2\mu_B$ in Fe_3Si due to the high position of the V level.

IV. RESULTS OF LMTO-CPA CALCULATIONS FOR $Fe_{3+y}Si_{1-y}$ AND $Fe_{3-x}V_xSi$

A. $Fe_{3+y}Si_{1-y}$

The d levels of Si[D] and Fe[B] lie at very different energies. Therefore, for the $Fe_{3+y}Si_{1-y}$ alloy, in which Si[D] is replaced by Fe[B] as y increases, we cannot apply simple schemes like the virtual-crystal approach (VCA) to obtain the electronic structure. The strong

TABLE I. Calculated iron and silicon moments (μ_B per atom) as well as the magnetization (total moment in μ_B per formula unit) for $Fe_{3+y}Si_{1-y}$ ($Fe_{1-x}Si_x$) alloys. The average number for nearest-neighbor Fe[A,C] atoms is denoted by $N^1_{Fe}[A,C]$. The compound corresponding to $y=0$ ($x=0.25$) is the ordered Fe_3Si alloy, whereas that with $y=1.0$ ($x=0$) is the bcc iron, viewed as the Fe_3Fe crystal with DO_3 structure.

			Moments				
x	y	$N^1_{Fe}[A,C]$	Fe[A,C]	Fe[B]	Fe[D]	Si[D]	Total
$\frac{4}{16}$	0	4	1.10	2.52		−0.08	4.63
			1.21[a]	2.49[a]		−0.08[a]	4.83[a]
$\frac{3}{16}$	$\frac{1}{4}$	5	1.38	2.43	2.29	−0.08	5.70
$\frac{2}{16}$	$\frac{1}{2}$	6	1.67	2.35	2.27	−0.12	6.77
$\frac{1}{16}$	$\frac{3}{4}$	7	1.85	2.27	2.23	−0.13	7.81
0	1	8	2.22	2.22	2.22	2.22	8.88

[a]Obtained from LMTO calculations for Fe_3Si with inclusion of combined correction (Ref. 17).

scattering on the D sublattice implies that this alloy is in the regime of the so-called split-band limit.[31] The CPA method is therefore well suited for calculations for this system.

The composition of the alloy may be specified through y in the formula $Fe_{3+y}Si_{1-y}$ or x in $Fe_{1-x}Si_x$ with $y=1-4x$. We have performed LMTO-CPA calculations for $x=\frac{4}{16}$ (ordered Fe_3Si), $x=\frac{3}{16}$, $\frac{2}{16}$, and $\frac{1}{16}$. In reality, the regime of DO_3-type structures corresponds to $0.10\leq x\leq 0.265$ according to Ref. 6. Thus, the alloy with $x=\frac{1}{16}$ ($y=\frac{3}{4}$) is outside this regime, but we nevertheless include it in the calculations in order to examine trends.

The moments calculated for the individual sites as well as the total moment (per formula unit) are given in Table I. In the row giving the values for $y=0$ (ordered Fe_3Si) the results for the LMTO-LSD crystal calculations[17] are also given. The slight difference between these and the CPA results is mainly due to the fact that the LMTO-CPA scheme applied here, contrary to the calculation of Ref. 17, did not include the so-called "combined correction" term.[32] Also, for the other "end component" bcc iron (Fe_3Fe), we obtain moments $2.22\mu_B$ per atom which agree with crystal calculations.[33] It should be noted that the moment $2.13\mu_B$ of bcc iron in Ref. 33, was calculated at the theoretical equilibrium volume which is slightly smaller than the volume (corresponding to the Wigner-Seitz radius 2.608 a.u.) assumed in the present work.

The result summarized in Table I shows that the theoretical Fe[B] is almost independent of y; it decreases slightly from $2.5\mu_B$ in Fe_3Si to the $2.22\mu_B$ in bcc iron. The Fe[A,C] moments vary linearly with x, cf. Table I or, more clearly, as shown in Fig. 4. Figure 4 shows the calculated moments as well as the concentration dependence of the Fe[A,C] moments as used by Niculescu *et al.*[1] in their phenomenological model for the description of experimental data. It is seen that our calculated moments, like the model, extrapolate to zero for $x=\frac{8}{16}$. In the limit towards the pure iron the CPA results behave differently from the model due to the difference in the slopes of the two lines in Fig. 4. While our calculations join smoothly to the bcc value for $x\rightarrow 0$, the model would lead to a kink in the Fe[A,C] moment versus the c curve.

Experimentally, neutron-scattering data[3] yield the following sublattice moments in Fe_3Si: Fe[A,C], $(1.2\pm0.12)\mu_B$; Fe[B], $(2.4\pm0.06)\mu_B$; and Si[D], $(-0.07\pm0.06)\mu_B$. Similar measurements by Moss and Brown[4] yield $1.07\pm0.06\mu_B$, $2.23\pm0.06\mu_B$ for the Fe[A,C] and Fe[B] moments. The saturation magnetization measurements of Ref. 5 are in reasonably good agreement with these results: Fe[A,C]; $1.35\mu_B$; Fe[B], $2.2\mu_B$; Si[D], $-0.07\mu_B$. The total moment $4.83\mu_B$, as well as the sublattice moments derived from the LMTO

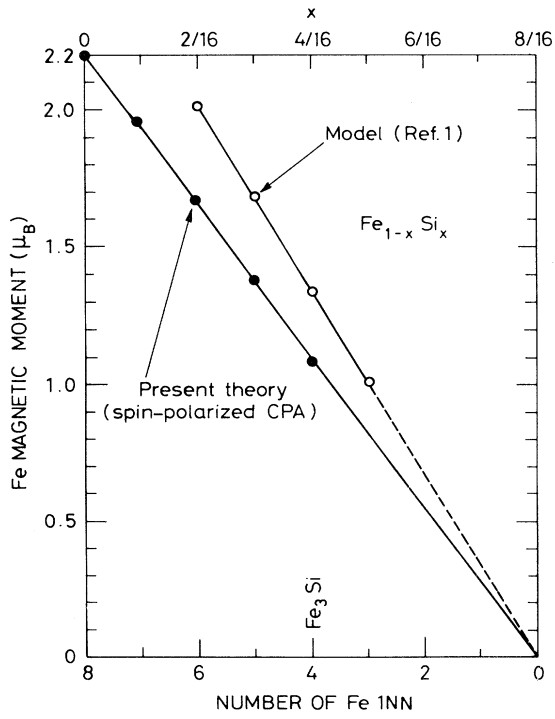

FIG. 4. $Fe_{3+y}Si_{1-y}$ ($Fe_{1+x}Si_x$). Magnetic moment of iron on the A and C sites as a function of composition x or N^1_{Fe}, the number of Fe 1NN.

calculations with combined correction, agree very well with the experiments, in particular, those of Ref. 3. The LMTO-CPA results (where the combined correction term is omitted) are slightly worse, but considering the spread in the experimental values quoted above, these also agree satisfactorily with observations. Note that even the small, negative Si moment has been found experimentally.[3,5]

The calculated DOS functions are shown in Figs. 5–7. First we note, by comparing the sublattice DOS functions for $x=0.25$ of Figs. 6 and 7 to the calculations for crystalline Fe_3Si in the preceding section, that the CPA calculations reproduce the characteristic features of the Fe[B] and Fe[A,C] DOS. The CPA calculations lead to DOS functions with less fine structure (due to the lower-energy resolution, a coarse **k** mesh, and the method of analytical deconvolution[23] also used for the calculations for the ordered phase), but the two-peak structure of the Fe[B] and the three-peak structure of the Fe[A,C] DOS are clearly resolved. Also, as was mentioned in Refs. 17 and 28, the Fe[B] majority-spin DOS (solid line in the upper part of Fig. 7) *is* somewhat different in shape from the minority DOS; the t_{2g} antibonding peak is more clearly separated from the e_g nonbonding peak, revealing the inherent three-peak structure of the Fe[B] DOS. The DOS functions in the other end of the composition range considered ($x=0.0625$, $y=0.75$) show that the Fe[B], Fe[D], as well as Fe[A,C], DOS functions approach the shapes characteristic[26–28] for pure bcc iron. This is most clearly seen from the figures at the bottom of Figs. 6 and 7, from which it also follows "at a glance" that the polarization of pure iron[25] must be $\approx 2\mu_B$.

For intermediate compositions x, we find that the Fe[B] DOS depends only weakly on the Si content. The local Fe[D] DOS behaves somewhat similarly but exhibits a more pronounced dependence on x. The Fe[A,C] local DOS, on the other hand, varies significantly upon alloying as the average number of Fe atoms in the 1NN (nearest-neighbor) shells around Fe[A,C] decreases from 7 for $x=0.0625$ to only 4 in the Fe_3Si crystal. The Fe[A,C] DOS changes from the bcc two-peak structure ($x=0.0625$) to the three-peak Fe[A,C] DOS in Fe_3Si.

The low-lying peaks around -0.70 Ry are due to Si. This is seen by their growth in intensity with Si content

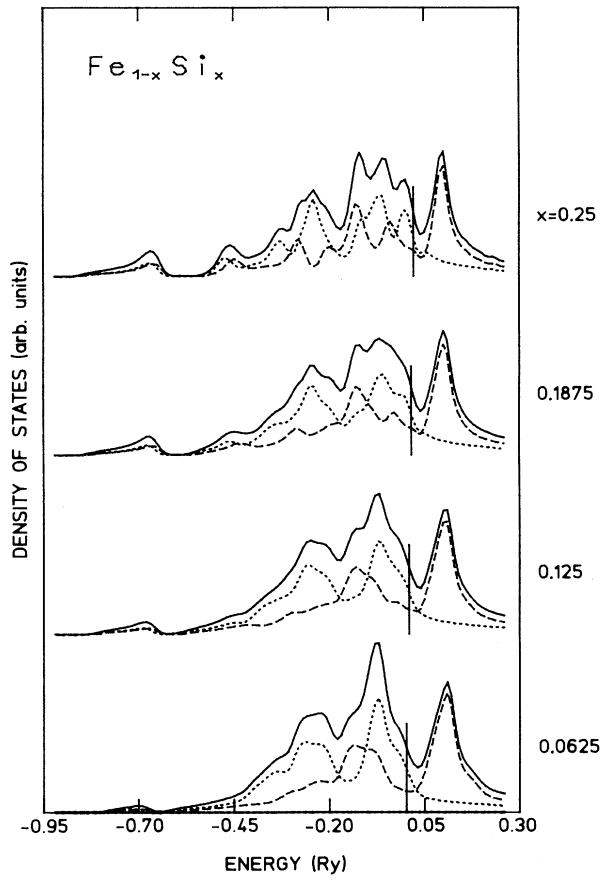

FIG. 5. $Fe_{3+y}Si_{1-y}$ (or $Fe_{1+x}Si_x$). Total density-of-states (DOS) functions (solid lines) and decompositions into majority-spin (dashed) and minority-spin (dotted) DOS functions. The vertical lines indicate the Fermi levels.

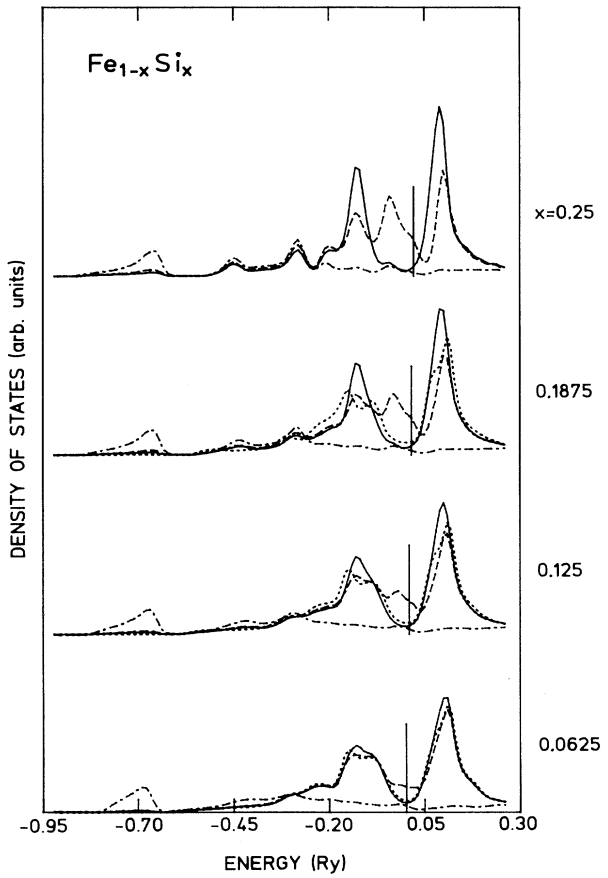

FIG. 6. $Fe_{3+y}Si_{1-y}$ (or $Fe_{1+x}Si_x$). Atom-projected minority-spin DOS functions: Fe[B] (solid lines), Fe[A,C] (dashed), Fe[D] (dotted), and Si[D] (dot-dashed).

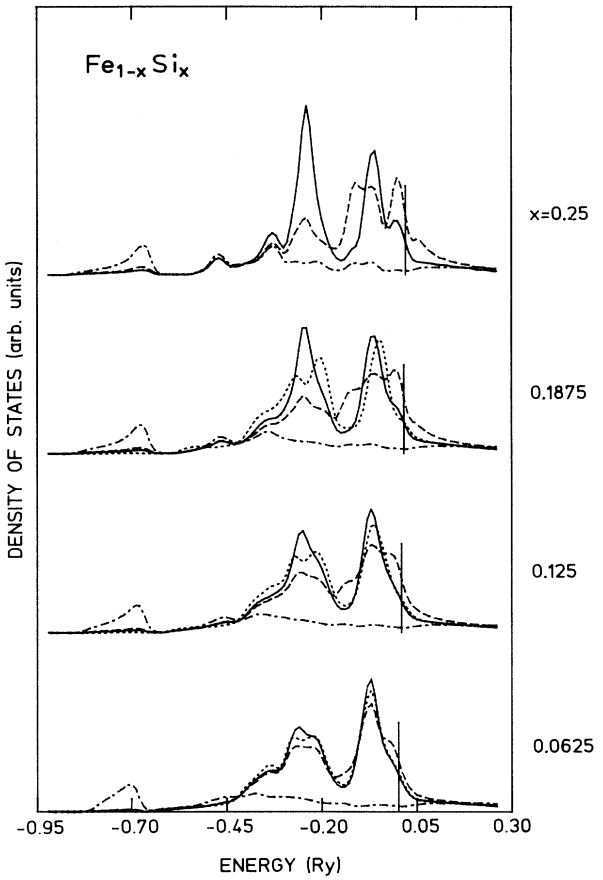

FIG. 7. The same as Fig. 6, but for majority spin.

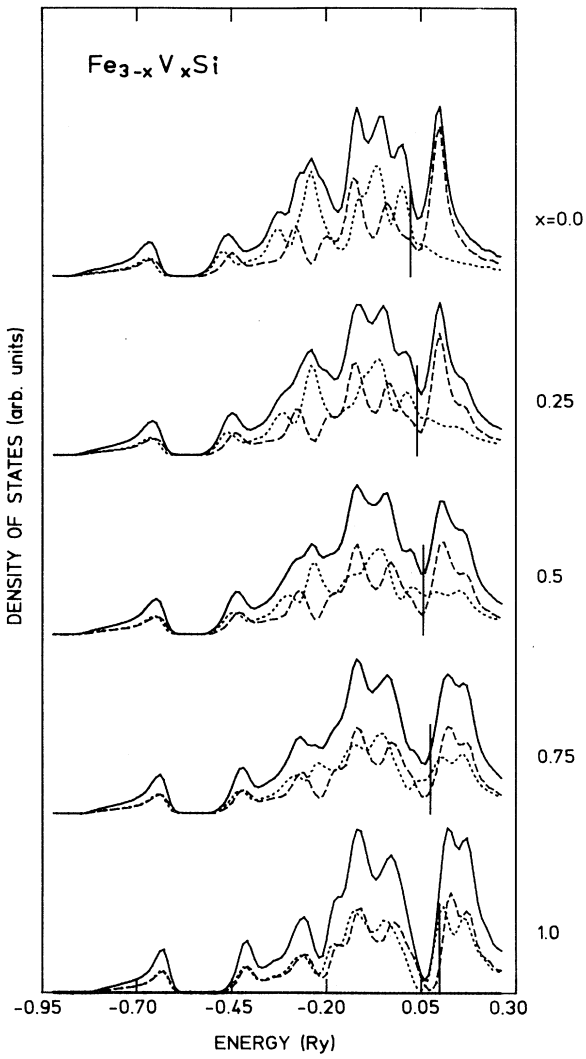

FIG. 8. $Fe_{3-x}V_xSi$. Total (solid lines) minority-spin (dashed) and majority-spin (dotted) DOS functions. The Fermi-level positions are indicated by vertical lines.

in Fig. 5, and clearly from the site projections in Figs. 6 and 7. The shape of the Si DOS changes only slightly with composition, and the up and down Si DOS are almost coinciding, a fact that reflects the small size of the Si moment.

B. $Fe_{3-x}V_xSi$

The DOS functions derived from the CPA calculations for $Fe_{3-x}V_xSi$ with x in the range $0 \leq x \leq 1.0$ are shown in Figs. 8–10, and the calculated moments are listed in Table II. As discussed in Sec. IV A, the CPA-derived DOS for Fe_3Si agrees well with the crystal calculation. We also find for the other end compound, Fe_2VSi, CPA DOS in good agreement with the results of the LMTO calculations[17] for the ordered Fe_2VSi.

From the total DOS for majority and minority spins in Fig. 8, we see that the Fermi level (indicated by a vertical bar) moves to higher energies with increasing x. This trend is opposite to what one would have expected from a rigid-band picture, and it points to the significant changes of band shapes occurring upon alloying. The decrease of the (total) magnetic moment with increasing x manifests itself in the fact that the majority- and minority-spin DOS functions become increasingly similar. The site- and spin-projected DOS are shown in Figs. 9 and 10. As in the previous case, the Si DOS is small, fairly independent of the spin, and hardly changing upon alloying. Its most prominent features are the Si s-like low-energy peak at -0.65 Ry and two peaks around -0.40 and -0.30 Ry; these contribute to the binding between Si and Fe[A,C].

The transition-metal projected DOS functions contain the characteristic features which were discussed in some detail in Sec. III. There it was argued that, in Fe_2VSi, the Stoner I for V is not large enough to spin polarize the e_g peak, and V gets a small moment directed opposite the Fe moment. The Fe[A,C] moment itself is small, $0.37\mu_B$, as compared to that of Fe_3Si, $1.2\mu_B$. As we now substitute part of the V atoms on the B sites by Fe, we create a level on these B sites which is essentially in resonance with the levels at the neighboring A and C sites. The Fe[B] level

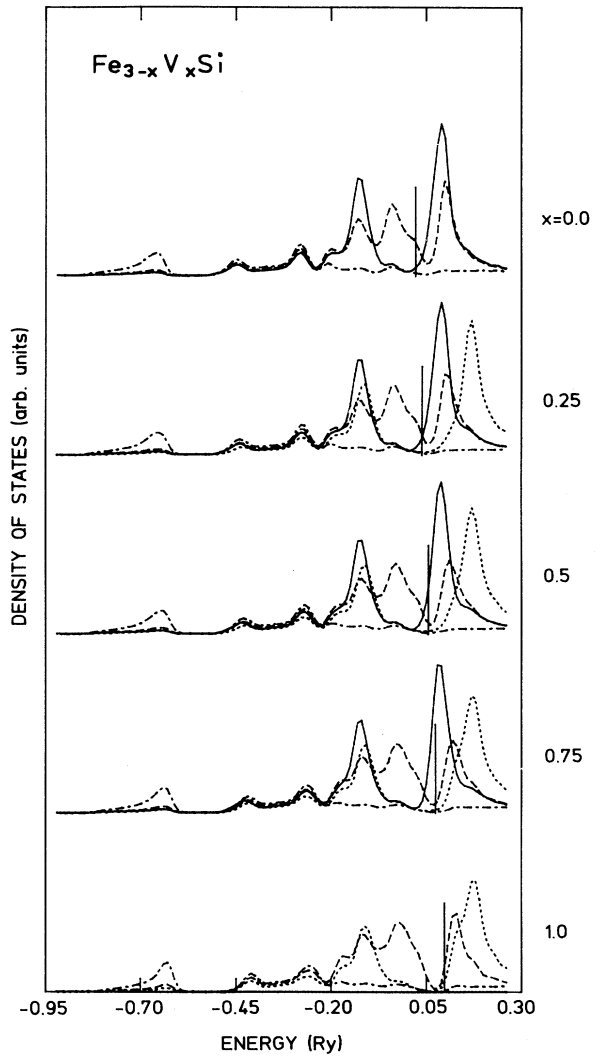

FIG. 9. Minority-spin DOS of $Fe_{3-x}V_xSi$: Fe[B] (solid lines), Fe[A,C] (dashed), V[B] (dotted), and Si[D] (dot-dashed).

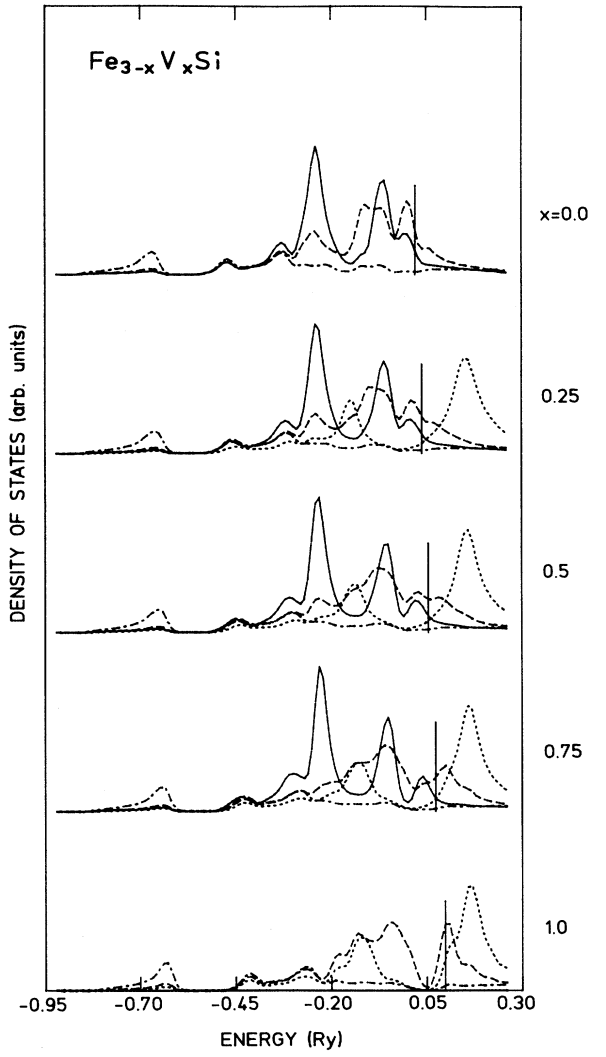

FIG. 10. The same as Fig. 9, but for majority spin.

is, however, strongly spin split, and the interaction between the Fe[B] orbitals and those on the neighboring Fe[A,C] sites induces increased spin polarization on the latter sites. The minority bonding Fe t_{2g} peak happens to coincide in energy with that of V so that interactions through common Fe[A,C] orbitals lead to an increased antiferromagnetic V moment.

The analysis above explains the trends observed in the

TABLE II. Calculated moments (μ_B per atom) and the magnetization (total moment in μ_B per formula unit) for $Fe_{3-x}V_xSi$ alloys. $N^1_{Fe}[A,C]$ is the average number of Fe atoms in the first nearest-neighbor shell, A or C site.

		Moments				
x	$N^1_{Fe}[A,C]$	Fe[A,C]	Fe[B]	V[B]	Si[D]	Total
0.0	4	1.10	2.52		−0.08	4.63
		1.21[a]	2.49[a]		−0.08[a]	4.83[a]
0.25	3	0.83	2.50	−0.23	−0.07	3.41
0.50	2	0.64	2.43	−0.16	−0.05	2.35
0.75	1	0.47	2.10	−0.10	−0.04	1.35
1.00	0	0.37		−0.03	−0.02	0.70

[a]These moments are obtained from LMTO calculations (for Fe_3Si) that include the combined correction term (Ref. 17).

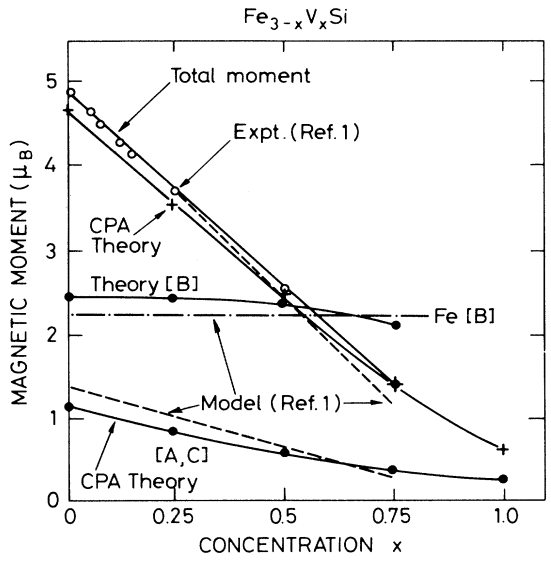

FIG. 11. $Fe_{3-x}V_xSi$. Calculated magnetic moments (present work, theory) and experimental (Ref. 1) data as well as their decomposition according to the local-environment model (Ref. 1) (dashed and dot-dashed straight lines). The open circles represent the measured total moments.

moments listed in Table II for $Fe_{3-x}V_xSi$. The Fe[B] moments stay roughly x independent, Fe[B] being "bcc-Fe-like," the Fe[A,C] moments decrease with x, and so does the average B-site moment. Also, the total moment decreases with x. Quantitatively, these concentration variations agree very well with experiments,[1] considering the total moment, and with the decomposition of experimental data as performed by means of the model of Ref. 1. This can be seen from Fig. 11. The moment variations in the range $0 \leq x \leq 0.75$ are all almost linear but the experimental total moment shows as a small departure from linearity (dashed curve). The calculated total-moment curve exhibits a small nonlinear shift in the same direction. Disregarding very fine details, the present LMTO-CPA calculations are seen to agree extremely well with the phenomenological model of Niculescu *et al.*[1]

V. CONCLUSIONS AND SUMMARY

A quantitative theory of electronic states in off-stoichiometric $Fe_{3+y}Si_{1-y}$ and $Fe_{3-x}V_xSi$ compounds, as presented here, requires the application of the CPA method. The main reason why simpler approximations are not applicable is that the d levels of Fe, V, and Si are at very different energies so that these alloys are in the split-band regime. The *ab initio* calculations, which are performed here by means of a scheme that combines the LMTO method with the CPA, include spin polarization, within the local approximation to density-functional theory, and allows the calculation of magnetic moments as functions of alloy composition. The method has recently been applied to binary alloys but here it is extended to the case of ternary systems.

The calculated moments do not only agree with experimental values but the composition dependence found for the sublattice moments also confirms the local-environment model used by Niculescu *et al.*[1] in their analysis of experimental results. For the end compounds, the CPA calculations yield sublattice moments that agree with neutron-scattering data as well as with self-consistent traditional crystal LMTO-LSD calculations.

The Fe atoms on B sites, which in Fe_3Si have cubic symmetry, have essentially the same moments as in bcc, Fe, and the Fe[B] DOS has a characteristic two-peak structure. The Fe[A,C] moments which, in contrast to the Fe[B] moments, vary markedly with composition, are induced by interactions with the Fe[B] orbitals. The Fe[B] DOS, the B sites having tetrahedral symmetry, has the three-peak shape. Arguments, in the spirit of the frozen-potential method, explain the remarkable site preference observed for $3d$ transition-metal impurities in Fe_3Si in terms of the differences between the shapes of the Fe[B] and Fe[A,C] DOS functions i.e., a difference that is traced back to the different point symmetry of these sites in the DO_3 structure.

*Permanent address: Institute of Physics, Czechoslovak Academy of Sciences, Na Slovance 2, 18040 Praha, Czechoslovakia.

†Also at: Institute of Physics, Aarhus University, DK-8000 Aarhus C, Denmark.

[1]V. A. Niculescu, T. J. Burch, and J. I. Budnick, J. Magn. Magn. Mater. **39**, 223 (1983).

[2]P. J. Webster and K. R. A. Ziebeck, in *Landolt-Börnstein, New Series,* edited by H. P. J. Wijn (Springer-Verlag, Berlin, 1988), Vol. 19c.

[3]A. Paoletti and L. Passani, Nuovo Cimento **32**, 1449 (1964).

[4]J. Moss and P. J. Brown, J. Phys. F **2**, 358 (1972).

[5]W. A. Hines, A. H. Menotti, J. I. Budnick, T. J. Burch, T. Litrenta, V. Niculescu, and K. Raj, Phys. Rev. B **13**, 4060 (1976).

[6]M. Hansen, *Constitution of Binary Alloys* (McGraw-Hill, New York, 1958).

[7]V. Niculescu, H. Raj, J. I. Budnick, W. A. Hines, and A. H. Menotti, Phys. Rev. B **14**, 4160 (1976).

[8]T. J. Burch, T. Litrenta, and J. I. Budnick, Phys. Rev. Lett. **33**, 421 (1974).

[9]S. Pickart, T. Litrenta, T. J. Burch, and J. I. Budnick, Phys. Lett. A **53**, 321 (1975).

[10]C. Blaauw, G. R. Mackay, and W. Leiper, Solid State Commun. **18**, 729 (1975).

[11]J. I. Budnick, Zhengquan Tan, and D. M. Pease, Physica B **158**, 31 (1988).

[12]A. C. Switendick, Solid State Commun. **19**, 511 (1976).

[13]S. Ishida, I. Ishida, S. Asano, and J. Yamashita, J. Phys. Soc. Jpn. **41**, 1570 (1976).

[14]A. R. Williams, V. L. Moruzzi, C. D. Gelatt, J. Kübler, and K. Schwartz, J. Appl. Phys. **52**, 2099 (1982).

[15]E. J. D. Garba and R. I. Jacobs, J. Phys. F **16**, 1485 (1986).
[16]S. Ishida, S. Fuji, N. Shimura, and S. Asano, J. Phys.: Condens. Matter **1**, 5115 (1989).
[17]N. E. Christensen, J. Kudrnovský, and O. K.. Andersen (unpublished).
[18]O. K. Andersen and O. Jepsen, Phys. Rev. Lett. **53**, 2571 (1984); O. K. Andersen, O. Jepsen, and D. Glötzel, in *Highlights of Condensed-Matter Theory,* Proceedings of the International School of Physics "Enrico Fermi," Course 89, Varenna, 1985 edited by F. Bassani, F. Fumi, and M. P. Tosi (North-Holland, New York, 1985); O. K. Andersen, O. Jepsen, and M. Šob, in *Electronic Band Structure and Its Applications,* edited by M. Yussoff (Springer-Verlag, Berlin, 1987), p. 1.
[19]J. Kudrnovský, V. Drchal, and J. Mašek, Phys. Rev. B **35**, 2487 (1987).
[20]J. Kudrnovský and V. Drchal, Phys. Rev. B **41**, 7515 (1990).
[21]V. A. Niculecu and J. I. Budnick, Solid State Commun. **24**, 631 (1977).
[22]S. K. Bose, J. Kudrnovský, M. van Schilfgarde, P. Blöchl, O. Jepsen, M. Methfessel, A. T. Paxton, and O. K. Andersen, J. Magn. Magn. Mater. (to be published).
[23]K. C. Hass, B. Velický, and H. Ehrenreich, Phys. Rev. B **29**, 3697 (1984).
[24]R. A. Tawil and J. Callaway, Phys. Rev. B **7**, 4242 (1973).
[25]The Fermi level of the (nonpolarized) band structure of bcc iron falls at the very strong peak of the DOS. A LDA-Stoner analysis (Refs. 26–28) shows that the peak is so narrow that it polarizes fully, i.e., the difference between the number of majority and minority spins becomes (approximately) 2. Consequently, the moment is $\approx 2\mu_B$.
[26]U. K. Poulsen, J. Kollár, and O. K. Andersen, J. Phys. F **6**, L241 (1976).
[27]O. K. Andersen, J. Madsen, U. K. Poulsen, O. Jepsen, and J. Kollár, Physica B **86-88**, 249 (1977).
[28]See, in particular, *Highlights of Condensed-Matter Theory,* O. K. Andersen, O. Jepsen, and D. Glötzel, in Proceedings of the International School of Physics "Enrico Fermi," Course 89 Varenna, 1985, edited by F. Bassani, F. Fumi, and M. P. Tosi (North-Holland, New York, 1985).
[29]This turns out to be rather crude—the majority DOS of Fe[B] in Fe_3Si does differ in shape from the minority DOS, the e_g nonbonding and t_{2g} antibonding peaks being somewhat more separated in energy (Ref. 17).
[30]O. K. Andersen and N. E. Christensen (unpublished); see also, N. E. Christensen and O. B. Christensen, Phys. Rev. B **33**, 4739 (1986).
[31]H. Ehrenreich and L. M. Schwartz, Solid State Phys. **31**, 149 (1976).
[32]O. K. Andersen, Phys. Rev. B **12**, 3060 (1975). The combined correction term corrects the finite angular-momentum cutoff in the partial-wave expansions and for the nonspherical shape of the atomic cells.
[33]N. E. Christensen, O. Gunnarsson, O. Jepsen, O. K. Andersen, J. Phys. Colloq. **49**, Suppl. C8-17 (1988), and references therein.